Forestry Research

ARTICLE

Open Access

https://doi.org/10.48130/forres-0026-0033

Forestry Research **2026**, 6: e031

PLASMODESMATA-LOCATED PROTEIN 6 regulates lateral symplastic transport during stem secondary growth in *Populus*

Renhui Li[1,2#], Hang Qin[1,3#], Wenjing Hu[1,2], Kexin Luan[1,2], Jiayan Sun[1], Junhui Shen[1] and Laigeng Li[1*]

[1] *The Key Laboratory of Plant Carbon Capture, CAS Center for Excellence in Molecular Plant Sciences, Chinese Academy of Sciences, Shanghai 200032, China*
[2] *University of the Chinese Academy of Sciences, Beijing 100049, China*
[3] *Department of Urology, The First Affiliated Hospital of Xi'an Jiaotong University, Shaanxi 710061, China*
[#] Authors contributed equally: Renhui Li, Hang Qin
[*] Correspondence: lgli@cemps.ac.cn (Li L)

Abstract

Secondary growth in trees results in an increase in stem diameter, which requires lateral transport of photoassimilates to the xylem for cell wall biosynthesis. However, how this lateral transport occurs during secondary growth remains poorly understood. We identified two PLASMODESMATA-LOCATED PROTEIN (PDLP) genes, *PdPDLP6A* and *PdPDLP6B*, in *Populus*, which are preferentially expressed in stem secondary growth tissues. Editing of both genes promoted cambial division and xylem development. PdPDLP6A and PdPDLP6B localize to plasmodesmata and modulate symplastic transport, consistent with a role in lateral transport from phloem to xylem across the stem. These findings suggest that PdPDLP6-modulated symplastic transport plays important roles in stem secondary growth in *Populus*.

Keywords: Secondary growth, Xylem, Plasmodesmata, Vascular cambium, Cell walls

Citation: Li R, Qin H, Hu W, Luan K, Sun J, et al. 2026. PLASMODESMATA-LOCATED PROTEIN 6 regulates lateral symplastic transport during stem secondary growth in *Populus*. *Forestry Research* 6: e031 https://doi.org/10.48130/forres-0026-0033

Introduction

Perennial trees grow and develop through two main processes. Primary growth, driven by apical meristems, produces upward elongation. Secondary growth, driven by the vascular cambium, leads to an increase in stem diameter[1,2]. Secondary growth requires photoassimilate transport to the xylem for cell wall biosynthesis via symplastic and apoplastic pathways[3–5]. Plasmodesmata (PD) form symplastic channels that mediate the movement of diverse molecules, including photoassimilates, proteins, and microRNAs[6–9]. Transport through PD is dynamically regulated by deposition and removal of callose at PD[10]. Excessive deposition of callose at PD can block or narrow the channels, thereby reducing their conductance[11]. Callose synthases (CALSs) and β-1,3-glucanases (BGs), members of glycosyl hydrolase family 17 (GH17), mediate synthesis and hydrolysis of callose, respectively[10]. During the stem's secondary growth, PD plays a role in symplastic transport across the phloem, vascular cambium, and xylem[12]. However, how symplastic transport operates during stem secondary growth remains poorly understood.

The PD-located proteins (PDLPs), which guide callose accumulation at PD, are widely recognized as key regulators of PD conductance[13,14]. The *Arabidopsis* genome contains eight PDLPs, PDLP1 to PDLP8, which are type I membrane proteins containing a signal peptide, two domains of unknown function 26 (DUF26), and a transmembrane domain with a short cytoplasmic tail[15]. *Arabidopsis* PDLP5 modulates auxin accumulation, and its mutant exhibits increased lateral root primordia formation[16]. PDLP6 forms a protein complex with SUS6 and CALS7, affecting sucrose transport from leaves to other tissues[13].

In this study, we identified two *Populus PDLP6* genes, which are preferentially expressed during stem secondary growth. Genetic, cellular, and biochemical analyses suggest that *PdPDLP6A* and its homolog *PdPDLP6B* function redundantly in regulating secondary growth. Our results indicate that PdPDLP6A and PdPDLP6B regulate PD conductance to modulate symplastic transport across the stem and suggest that these proteins play important roles in symplastic trafficking during secondary growth in *Populus*.

Materials and methods

Plant growth

Populus deltoides × *Populus euramericana* cv. Nanlin895 was used in this study. The *Populus* trees were grown for 2 months in a phytotron under the following conditions: a 14-h light/10-h dark photoperiod, 60% relative humidity, and a temperature of 25 °C.

Stem diameter was measured at the 10th internode using a Vernier caliper. Measurements were taken from six independent biological replicates per line.

Biomass quantification

Debarked stems were dried at 70 °C for 7 d, and the dry weight was measured for biomass assessment. Measurements were taken from four independent biological replicates per line.

Gene sequence analysis

The amino acid sequences of PDLP proteins were obtained from the *Populus* genome database (https://phytozome-next.jgi.doe.gov/info/Ptrichocarpa_v4_1) and the *Arabidopsis* Biological Resource Center (www.arabidopsis.org). The phylogenetic relationship was analyzed in MEGA 6.0 using the neighbor-joining method[17]. Bootstrap values were calculated from 1,000 replicates. Protein domain analysis was performed using the SMART database (https://smart.embl.de).

© The Author(s)

https://doi.org/10.48130/forres-0026-0033

Gene cloning, constructs, and transformation

'Nanlin895' was used for gene cloning and genetic transformation. According to the sequences of *Potri.010G108100* and *Potri.008G133500* identified in the *Populus trichocarpa* genome, their corresponding cDNAs were cloned from 'Nanlin895' and named *PdPDLP6A* and *PdPDLP6B*, respectively. For construction of overexpression vectors, the full-length CDSs of *PdPDLP6A* and *PdPDLP6B* were separately cloned into the *pCAMBIA2300* vector under the control of the *CaMV 35S* promoter. For construction of the *CRISPR/Cas9* vectors, gene-specific target sequences of *PdPDLP6A* and *PdPDLP6B* were assembled into sgRNA expression cassettes and then subcloned into a *pYLCRISPR/Cas9P35S-H* plasmid as described in Ma et al.[18]. The transformation was carried out according to the protocol used in our lab[19]. For the subcellular localization assay, the *PdPDLP6A/6B-Gly-Ser* linker cassettes were cloned into *pHB-35S:YFP* vectors in frame with YFP. Primers used for vector construction are listed in Supplementary Table S1.

RNA extraction, qRT-PCR analysis, and RNA sequencing

Total RNA was isolated from various *Populus* tissues using the FastPure Universal Plant Total RNA Isolation Kit (Vazyme Biotech, RC411-01) according to the manufacturer's instructions. cDNA was generated using the cDNA Synthesis SuperMix (TransGen Biotech, AT311-03). Quantitative reverse transcription PCR (qRT-PCR) was carried out on a QuantStudio 3 Real-Time PCR System (Applied Biosystems) using PerfectStart Green qPCR SuperMix (TransGen Biotech). *ACT2* was used as an endogenous reference for normalization. Primers used in the study are listed in Supplementary Table S1. For analysis of *PDLP6* expression in different organs or stem tissues, three biological replicates of WT plants were used. For gene overexpression in the stem of transgenic plants, stem segments from the 12th internode were collected from three biological replicates of WT and transgenic plants.

For RNA sequencing (RNA-seq), two biological replicates of WT and *pdlp6ab* mutant were analyzed. The 12th internode stems were cut into 2 mm segments and used for total RNA extraction. A cDNA library was generated from 5 μg of total RNA with the Illumina® Stranded mRNA Prep kit. The cDNA library was assessed for fragment-size distribution using an Agilent 2100 Bioanalyzer. Paired-end 150-bp sequencing was performed on an Illumina NovaSeq X Plus platform. Raw sequencing reads were processed with Trim Galore to remove adapter sequences and low-quality bases. The resulting high-quality reads were mapped to the *P. trichocarpa* reference genome v4.1 (Joint Genome Institute Phytozome database) using HISAT2. Gene-level read counts were generated from the alignment files using featureCounts with the corresponding gene annotation. Differential expression analysis was performed using the DESeq2 package in R, comparing the *pdlp6ab* mutant with WT samples. *p*-Values were adjusted using the Benjamini–Hochberg procedure, and genes with an adjusted p value < 0.05 and an absolute $\log_2$ fold change > 1 were considered significantly differentially expressed. Gene Ontology (GO) functional enrichment analysis of the differentially expressed genes was performed using the DAVID Bioinformatics Resources.

Stem anatomy and cell wall observation

The 13th internodes from five biological replicates per line were cut into 2 mm segments and vacuum-infiltrated in FAA fixative (formaldehyde : glacial acetic acid : ethanol = 1:1:18) for 2 h, followed by 24 h incubation at 4 °C. After dehydration through an ethanol concentration series (70%, 80%, 95%, 100%; 1 h per step), samples were cleared in ethanol-xylene (1:1, 1 h) and pure xylene (1 h, two times), then infiltrated with xylene-paraffin (1:1, 1 h) and pure paraffin (12 h) at 70 °C, and finally embedded in fresh paraffin and stored at 4 °C. The 12 μm sections were cut using a Leica RM2235 rotary microtome. The sections were deparaffinized in xylene, stained with 0.05% toluidine blue, and observed under an Olympus BX53 light microscope.

For examination of cell wall thickness, the 14th internode of 2-month-old plants was cut into 1 mm^3 pieces and immersed in fixation buffer (0.1 mol/L PBS, pH 7.4, with 0.5% glutaraldehyde). The sample was fixed in 0.5% osmic acid before being dehydrated and embedded in LR white resin (Polysciences, Warrington, PA, USA). Uranyl acetate and lead citrate were used to stain ultrathin sections. Cell wall ultrastructure was observed using a transmission electron microscope (H-7650; Hitachi, Kyoto, Japan) as described previously[20], and cell wall thickness was quantified using ImageJ.

Subcellular localization of PdPDLP6 and callose

The constructs of *pHB-PdPDLP6A* and *PdPDLP6B-YFP* were created and agroinfiltrated into *Nicotiana benthamiana* leaves as described previously[21]. After 48–60 h, the YFP signal was excited at 514 nm, and the emitted light was captured at 505 to 555 nm. Callose was stained with aniline blue; fluorescence was excited at 405 nm, and emission was detected at 460–500 nm as described[22]. The fluorescence signal was observed under a confocal microscope (Zeiss LSM880).

In *Populus,* stem cross-sections were stained for callose with 0.01% aniline blue and subsequently observed under an Olympus BX51 microscope. ImageJ software was used for callose quantification.

Symplastic passage analyses

Analysis of the TMV–GFP symplastic movement: The fifth leaf of 3-week-old *N. benthamiana* was infiltrated with *Agrobacterium tumefaciens* GV3101 transformed with an empty vector or *35S:PdPDLP6A/PdPDLP6B* plasmid as described previously[21]. After incubation for 48 h in the dark, the center of the infiltrated leaf was infiltrated with *A. tumefaciens* harboring *TMV–GFP*. After 5–7 d, TMV-GFP movement was visualized using a portable UV flashlight and photographed with a Nikon camera (NIKON D810).

Symplastic dye-tracing assay: Carboxyfluorescein diacetate (CFDA), a dye for tracing symplastic movement, was applied in the assay using the leaves of 1-month-old *N. benthamiana*. The adaxial side of the leaf was loaded with 1 μL of 1 mmol/L CFDA (Sigma-Aldrich) and incubated for 10 min. The leaf was then sectioned, and the CFDA signal on the abaxial side was observed using an Olympus BX51 microscope.

To examine the symplastic movement in *Populus*, the leaf at the 14th internode was removed while the petiole was retained. Then the petiole was immersed in a 1 mmol/L CFDA solution. After 12 h, cross-sections of the internode under the petiole were prepared and observed under a Zeiss LSM880 confocal microscope.

Determination of soluble sugar content in *Populus* stem

Fresh tissue (50 mg) from the 15th internode of 2-month-old plants was collected and rapidly frozen in liquid nitrogen, then ground into powder. Subsequently, the mixture of 1.4 mL methanol and tissue powder was vigorously vortexed and incubated at 70 °C with intermittent shaking to inactivate enzymes. After centrifugation at 14,000 × g for 3 min, the supernatant was transferred to a 15 mL tube, followed by the addition of 1.4 mL of water and 1 mL of

chloroform and thorough mixing. The mixture was centrifuged at 6,000 rpm for 15 min, and 500 μL of the upper polar phase was collected into a 1.5 mL EP tube. The sample was completely dried in a centrifugal concentrator. Next, 50 μL of mass spectrometry-grade BSTFA and 100 μL of mass spectrometry-grade pyridine were added, and the samples were incubated at 70 °C for 30 min. A 100 μL aliquot was transferred to a mass spectrometry vial for GC–MS analysis. For standard curve preparation, sucrose and glucose standards were mixed in a 1.5 mL EP tube at different concentrations, dried in a centrifugal concentrator, and processed identically to the samples for subsequent analysis. Three mutant lines (*pdlp6ab-1*, *pdlp6ab-2*, and *pdlp6ab-3*) were analyzed.

Esculin treatment

Esculin is a fluorescent sucrose analog used for live imaging of sugar transport[23]. The fully expanded leaf at the 12th internode of 2-month-old *Populus* was loaded with a 10 mg/mL esculin solution for 24 h. The internode immediately below the treated leaf was cross-sectioned. Esculin was excited at 405 nm, and emission was detected at 424–469 nm using a Zeiss LSM880 confocal microscope.

Cell wall composition analysis

Stems from the 15th–20th internodes were harvested from three independent biological replicates per line and were debarked. After being dried at 55 °C, the wood samples were ground to a fine powder and processed as alcohol-insoluble residues (AIRs) for analysis of monosaccharide composition and crystalline cellulose content, as described previously[24].

Staining for cell wall composition

The 14th internode of 2-month-old plants was manually cut into thin sections. Phloroglucinol was used to stain lignin, and Calcofluor White was used to stain cellulose. An Olympus BX51 light microscope was used for imaging.

Statistical analysis

All data are presented as mean ± standard deviation (SD) from at least three biological replicates, except for the RNA-seq experiment, which was performed with two biological replicates (two individual WT plants; two *pdlp6ab* mutant lines, one plant each). Statistical analyses were performed using GraphPad Prism 8.0.2 (GraphPad Software, San Diego, CA, USA). For comparisons between two groups, significance was determined by a two-tailed Student's t-test. For comparisons among multiple groups, one-way analysis of variance (ANOVA) was applied, followed by Dunnett's post-hoc test for comparisons against the WT or control. Significance levels are denoted as * $p < 0.05$ and ** $p < 0.01$. For the RNA-seq data, genes with an adjusted $p < 0.05$ (Benjamini–Hochberg correction) and $|\log_2$ fold change$| > 1$ were considered significantly differentially expressed.

Accession numbers

Sequence data are available in the Phytozome Database under the following accession numbers: *PdPDLP6A* (*Potri.010G108100*) and *PdPDLP6B* (*Potri.008G133500*). The sequences of *PdPDLP6A* and *PdPDLP6B* are provided in Supplementary Table S2.

Results

PdPDLP6A and *PdPDLP6B* are highly expressed in secondary vascular tissues

The secondary growth of stems depends on the supply of photoassimilates to xylem through symplastic and apoplasmic pathways[3–5]. PD provides the structural basis for the symplastic pathway. In our previous single-cell RNA sequencing (scRNA-seq) of stem tissue[25], a gene (*Potri.010G108100*) from the PDLP family was specifically expressed in tissues undergoing secondary growth in the stem. As the PDLP genes are recognized as important regulators of PD conductance[13,14,16], we sought to determine whether they contribute to stem secondary growth.

There are 10 putative *PDLP* homologs in the *Populus* genome compared with eight in *Arabidopsis* (Supplementary Fig. S1). *Potri.010G108100* is homologous to *Arabidopsis PDLP6* and has a close homolog (*Potri.008G133500*) in *Populus*. We cloned their corresponding cDNAs from *P. deltoides* × *P. euramericana* cv. 'Nanlin895' and named them *PdPDLP6A* and *PdPDLP6B*, respectively. Among them, *PdPDLP6A* showed the highest expression level in secondary growth stems (Fig. 1a). Both genes were highly expressed in stem phloem and xylem but weakly expressed in other tissues, including epidermis, cortex, and pith (Fig. 1b, c), suggesting their involvement in stem secondary growth.

PdPDLP6A and *PdPDLP6B* affect stem secondary growth in *Populus*

To investigate the *PdPDLP6* function in the secondary growth of *Populus*, we generated PdPDLP6-overexpressing plants and PdPDLP6-edited mutants. For overexpression, *PdPDLP6A* and

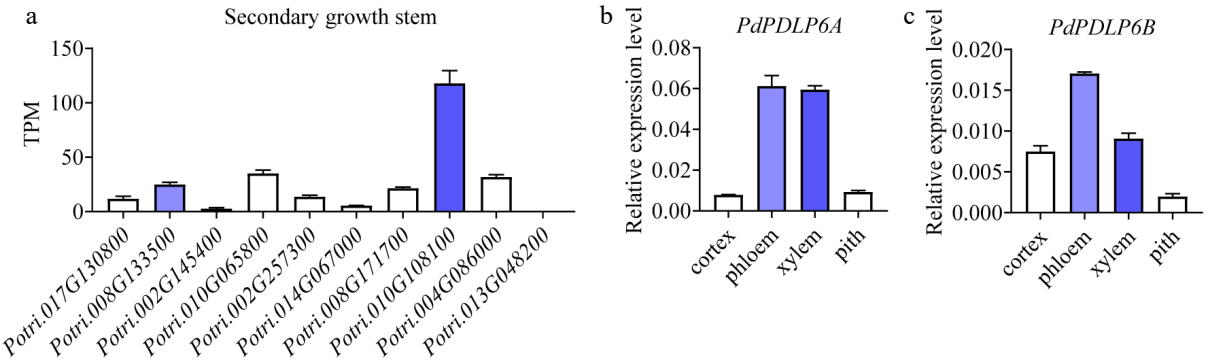


Fig. 1 *PdPDLP6A* was highly expressed in the vascular tissues of the secondary-growth stem. (a) Relative expression of *PdPDLPs* in secondary-growth stems based on our previously published RNA-seq data. TPM, transcripts per million. Values are means ± SD, $n = 3$. (b), (c) Relative expression of *PdPDLP6A*/*6B* in vascular tissues determined by qRT-PCR. Values are means ± SD, $n = 3$.

https://doi.org/10.48130/forres-0026-0033

PdPDLP6B were overexpressed individually under the control of the *35S* promoter. *PdPDLP6A* and *PdPDLP6B* were edited using CRISPR/Cas9-mediated genome editing. Conserved sequences within the DUF26 domain of PdPDLP6A and PdPDLP6B were selected as CRISPR/Cas9 targets (Supplementary Fig. S2a). The overexpression and genome editing constructs (Supplementary Fig. S2b) were transferred into *P. deltoides* × *P. euramericana* 'Nanlin 895' to generate transgenic plants, which included single mutants (*pdlp6a-1*, *pdlp6a-2*, *pdlp6b-1*, and *pdlp6b-2*), double mutants (*pdlp6ab-1*, *pdlp6ab-2*, and *pdlp6ab-3*) (Supplementary Fig. S2c, S2d), and overexpression plants (*6AOE-1*, *6AOE-2*, *6BOE-1*, and *6BOE-2*) (Supplementary Fig. S3a). The overexpression plants did not show visible secondary growth phenotypes (Supplementary Fig. S3b–S3d). The single mutants pdlp6a-1, pdlp6a-2, pdlp6b-1, and pdlp6b-2 showed no clear effect on secondary growth (Supplementary Fig. S4a), and stem anatomy also showed few alterations in cambium and xylem development (Supplementary Fig. S4b, S4c). The double mutants *pdlp6ab-1*, *pdlp6ab-2*, and *pdlp6ab-3* showed increased stem secondary growth with a larger stem diameter compared with wild type (WT) (Fig. 2a–c). Consistent with the stem diameter phenotypes, the double mutants accumulated more wood biomass (Fig. 2d). The results suggest that *PdPDLP6A* and *PdPDLP6*B act redundantly in regulating stem diameter growth in *Populus*.

Stems from 2-month-old double mutants were sectioned to examine their cellular anatomy. Compared with WT, the double mutants showed increased width of both the xylem and the cambial zone (Fig. 3a–d), as well as more cell layers in these tissues (Fig. 3e, f). The results indicate that editing of *PdPDLP6A* and *PdPDLP6B* promoted stem diameter enlargement, likely by enhancing cambium proliferation and xylem differentiation.

PdPDLP6A and *PdPDLP6B* affect the thickening of wood cell walls

During stem secondary growth, most photoassimilates from leaves are transported to the xylem and incorporated into secondary cell walls (SCWs). SCW thickness is indicative of the accumulation of wood biomass. Anatomical analysis showed increased lignin deposition but reduced cellulose staining in the xylem of the double mutants (Fig. 4a, b). Fiber walls were thicker in the mutants, whereas vessel walls remained largely unchanged (Fig. 4c–e). Chemical measurements further showed that lignin increased by 16%–20%, cellulose decreased by 18%–23%, and xylose and mannose levels increased (Fig. 4f). These results suggest that *PdPDLP6A* and *PdPDLP6B* play a role in SCW thickening during xylem development.

PdPDLP6A and PdPDLP6B impede PD conductance

To determine the subcellular localization of PdPDLP6A and PdPDLP6B, we created YFP fusion constructs and transiently expressed them in tobacco epidermal cells. Callose, which is associated with plasmodesmata[26], was visualized by aniline blue staining. The YFP signal in the merged channel colocalized with the callose signal at cell walls, indicating that PdPDLP6A and PdPDLP6B localize to the plasmodesmata (Fig. 5a). The expression of PdPDLP6A or PdPDLP6B resulted in increased callose deposition relative to the control (Fig. 5b, c). Meanwhile, tobacco leaves were infiltrated with *Agrobacterium* carrying the fluorescence-labeled virus TMV-GFP. Compared with the empty vector, expression of PdPDLP6A or PdPDLP6B restricted virus spread through symplastic channels from the leaf to the apex (Fig. 5d). Furthermore, we used CFDA to trace how PdPDLP6A and PdPDLP6B influence symplastic conductance. When PdPDLP6A or PdPDLP6B was expressed in tobacco epidermal cells, CFDA movement via the symplastic system from the adaxial to the abaxial side was reduced, indicating that they inhibit such transport (Fig. 5e, f). These findings indicate that PdPDLP6A and PdPDLP6B are associated with callose deposition at PD and reduce symplastic conductance.

Editing of *PdPDLP6A* and *PdPDLP6B* changes PD conductance

To examine how PdPDLP6A and PdPDLP6B affect symplastic transport in *Populus*, we performed the CFDA transport assay on the *pdlp6ab* mutants. We loaded CFDA into the petioles and, after 12 h of treatment, sectioned the internode below the treated petiole to examine lateral CFDA movement into the xylem. Compared with

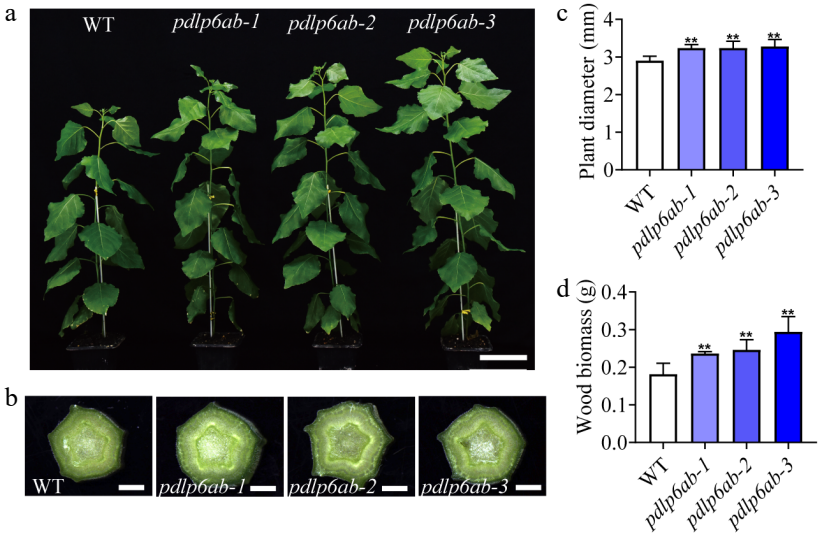


Fig. 2 *PdPDLP6A* and *PdPDLP6B* affect stem secondary growth. (a) Growth of WT and *pdlp6ab* double mutants. Scale bar = 10 cm. (b) Stem phenotypes of WT and *pdlp6ab* double mutants. Scale bar = 1 mm. (c) Stem diameter at the 10th internode. Values are means ± SD, $n = 6$, ** $p < 0.01$ (one-way ANOVA with Dunnett's test). (d) Xylem biomass of WT and *pdlp6ab* double mutants. Values are means ± SD, $n = 4$, ** $p < 0.01$ (one-way ANOVA with Dunnett's test).

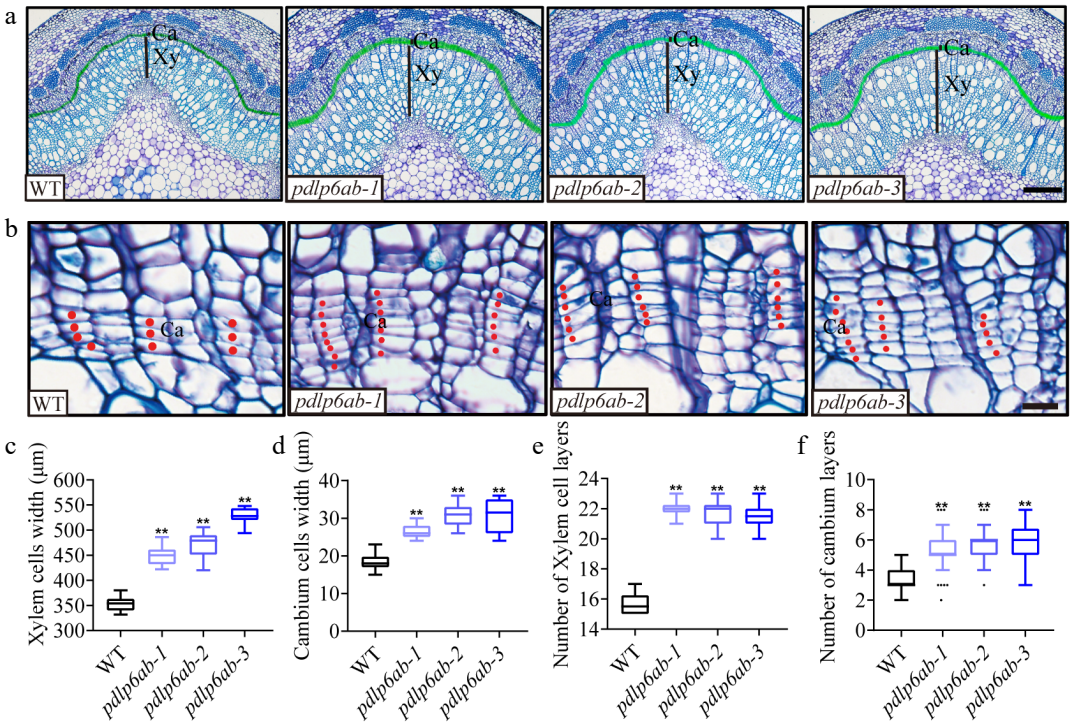


Fig. 3 *PdPDLP6A* and *PdPDLP6B* influence cambial division and xylem development. (a) Cross sections of the stems in the 13th internode stained with toluidine blue. Xy, xylem; Ca, cambium (indicated by the green shaded area). Scale bar = 200 μm. (b) Cross sections of the cambial zone. Red dots mark individual cambium cells. Ca, cambium. Scale bar = 20 μm. (c), (d) Width of xylem region and cambial zone. Values are means ± SD, $n = 5$, ** $p < 0.01$ (one-way ANOVA with Dunnett's test). (e), (f) Cell layer numbers of xylem and cambial zone. Values are means ± SD, $n = 5$, ** $p < 0.01$ (one-way ANOVA with Dunnett's test).

WT, the double mutants showed a stronger fluorescence signal in the xylem (Fig. 6a, b), suggesting that the *pdlp6ab* mutants had more CFDA transported to the xylem via the symplastic pathway. Parenchyma cells in the phloem and cambial zone showed weaker callose staining in the *pdlp6ab* mutants (Fig. 6c, d). The PD apertures of the double mutants appeared larger than those of WT (Supplementary Fig. S5). The results suggest that PdPDLP6A and PdPDLP6B influence the PD conductance across stems in *Populus*.

Sugar transport in the stem is altered in the *pdlp6ab* mutants

Given that photosynthates need to be transported to the xylem for biomass accumulation during stem secondary growth, we measured sucrose and glucose levels in the phloem and xylem. Compared with WT, the double mutants had similar sugar levels in the phloem but higher levels in the xylem (Fig. 7a). Using esculin, a fluorescent sucrose analog, we monitored sucrose transport. The double mutants showed stronger fluorescence signals in xylem regions than the WT, suggesting enhanced sugar transport to the xylem in the *pdlp6ab* mutants (Fig. 7b). RNA sequencing (RNA-seq) analysis revealed that differentially expressed genes (DEGs, Supplementary Table S3) between *pdlp6ab* and WT were enriched in pathways related to sucrose metabolism, carbohydrate metabolism, and secondary cell wall biogenesis (Fig. 7c). These data indicate that more sucrose was transported to the xylem in the *pdlp6ab* stems, which may have contributed to the enhanced xylem development and biomass accumulation. The RNA-seq data also showed significant changes in cell cycle-related genes, such as *CYCD3;3 and CYCD3;4*, suggesting an increased cambial division activity that is consistent with the increased number of xylem cell layers in the mutants[27,28] (Fig. 7d). Changes in the expression of genes related to sugar signaling and the cell cycle, including *HXK1*, *TOR*, and *CYCD3;3*, were confirmed in the mutants (Fig. 7e).

Discussion

PdPDLP6A and *PdPDLP6B* support a role in lateral symplastic transport and xylem development

During secondary growth in trees, photoassimilates unloaded from the phloem must move radially across the stem to support cell wall biosynthesis in the xylem. In trees, the xylem functions as a major sink for photoassimilates during stem secondary growth[12]. Previous studies showed that modifying PD conductance influences assimilate translocation from source to sink organs in rice and *Arabidopsis thaliana*[13,22]. These studies primarily examined photoassimilate transport from source tissues to developing seeds. How photoassimilates are transported into the xylem during stem secondary growth in trees remains poorly understood. Our results suggest that PdPDLP6 participates in radial symplastic transport and influences stem diameter growth in *Populus*. The two *PdPDLP6* homologs, *PdPDLP6A* and *PdPDLP6B*, are preferentially expressed in stem tissues. Single mutants of either *PdPDLP6A* or *PdPDLP6B* did not exhibit an obvious phenotype, whereas the double mutant displayed an increased number of xylem cell layers and more cell wall biomass accumulation. This suggests that the two *PdPDLP6* members may function redundantly in regulating stem secondary growth. Interestingly, their overexpression did not show clear phenotypic changes. This may reflect how PDLP6 functions. PDLP6 requires interaction with other factors to function[13]. Overexpression of PDLP6 alone may be insufficient to produce a detectable phenotype if the abundance or activity of its interacting partners is

https://doi.org/10.48130/forres-0026-0033

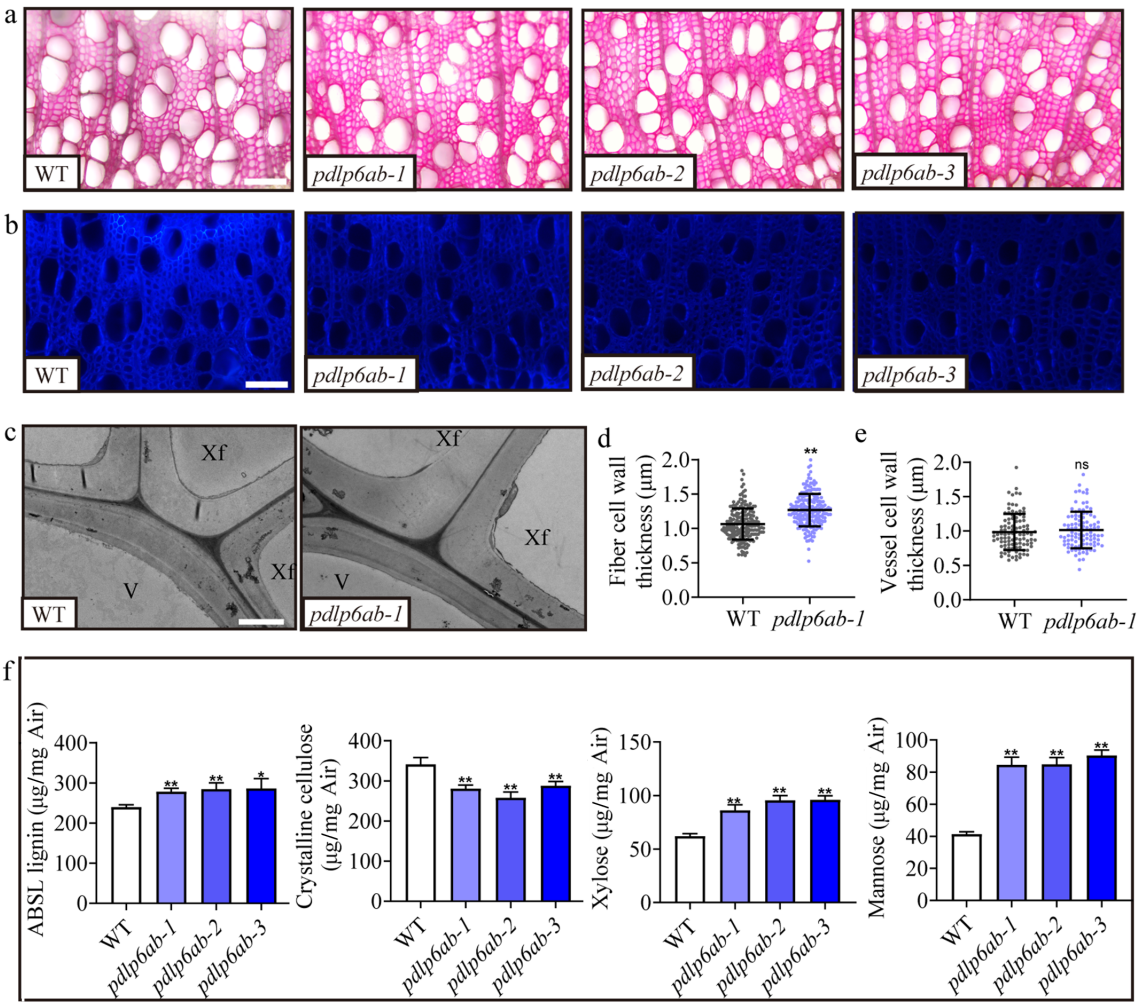


Fig. 4 *PdPDLP6A* and *PdPDLP6B* are involved in SCW thickening. (a) Cross sections of the stems in the 14th internode stained with phloroglucinol. Scale bar = 200 μm. (b) Cross sections of the stems at the 14th internode stained with Calcofluor White. Scale bar = 200 μm. (c) Transmission electron microscopy images of cell walls at the 14th internode. Scale bar = 2 μm. V, vessel; Xf, xylem fiber. (d) Quantification of xylem fiber and vessel cell wall thickness. Values are means ± SD, $n = 5$, ** $p < 0.01$ (Student's *t*-test). (e)–(f) Contents of cell wall components (lignin, cellulose, xylose, and mannose). Values are means ± SD, $n = 3$, ** $p < 0.01$ (one-way ANOVA with Dunnett's test).

limiting. Further study is needed to verify this hypothesis.

Our cellular and biochemical data indicate that editing of PdPDLP6A and PdPDLP6B alters symplastic transport in the stem, allowing more photoassimilates to reach the xylem sink and supporting increased cell wall biosynthesis. Furthermore, gene expression analysis showed that editing PdPDLP6A and *PdPDLP6B* induces changes in the expression of genes related to cell wall synthesis, cambium cell division, and sugar signaling. Together, these findings support a role for PdPDLP6A and PdPDLP6B in radial symplastic transport, a pathway that influences photoassimilate delivery to the xylem sink and thereby affects xylem development and biomass accumulation.

The increased sugar content in the xylem coincided with enhanced cambial activity and higher xylem biomass. The increased sugar availability may provide additional carbon for secondary cell wall biosynthesis. Concurrently, changes in stem sugar levels may activate signaling pathways that influence cambial activity to increase xylem cell layers. Previous studies suggest that glucose stimulates the expression of cell cycle genes to facilitate cell proliferation, likely through activation of TOR signaling[29,30]. In this study, gene-expression analysis showed changes in TOR signaling and cell-cycle-related genes, including *CYCD3;3* and *TOR*. The effects of PdPDLP6A and PdPDLP6B on xylem development and cell wall biomass accumulation may be associated with their influence on lateral symplastic sugar transport; however, the underlying mechanisms require further investigation.

PdPDLP6A and PdPDLP6B function in regulating plasmodesmata conductance

PDLPs are a family of proteins localized to plasmodesmata[10]. In *Arabidopsis*, it has been reported that PDLP5 interacts with GSL8[31] and PDLP6 interacts with CALS7[13] at plasmodesmata. Both GSL8 (CALS10) and CALS7 (GSL7) are plasmodesmata-localized callose synthases that control pore permeability and symplastic trafficking, thereby regulating intercellular communication during development[31,32]. Our findings suggest that PdPDLP6A and PdPDLP6B colocalize with callose at plasmodesmata, influencing plasmodesmal symplastic conductance; however, it remains uncertain whether their colocalization with callose is mediated by interactions with CALS or BG proteins in *Populus*. The mechanisms by which PdPDLP6 regulates plasmodesmal conductance require further investigation.

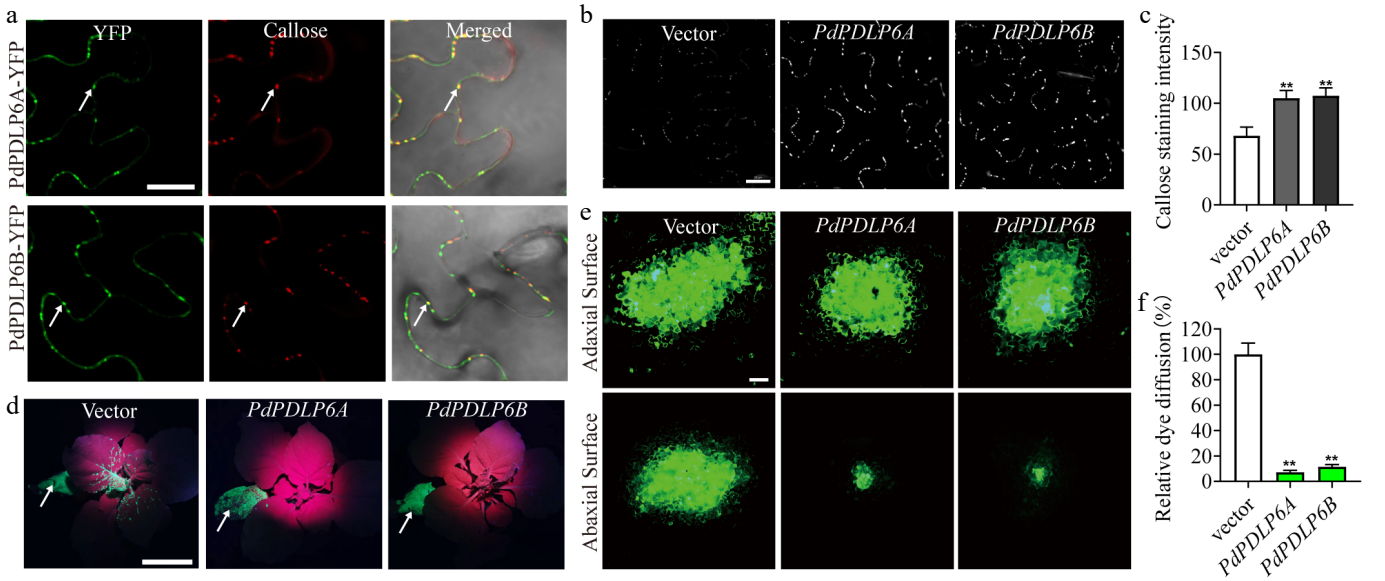


Fig. 5 PdPDLP6A and PdPDLP6B associate with callose at PD and reduce symplastic transport. (a) Subcellular localization of PdPDLP6A and PdPDLP6B. Callose is stained with aniline blue (red pseudocolor). Arrows point to sites of PdPDLP6A/6B and callose colocalization. Scale bar = 20 μm. (b) Punctate callose deposition detected by aniline blue staining, consistent with plasmodesmata localization. Scale bar = 20 μm. (c) Quantification of aniline blue fluorescence intensity in (b). Values are means ± SD, n = 5, ** p < 0.01 (one-way ANOVA with Dunnett's test). (d) TMV-GFP infiltration site (arrow). Expression of PdPDLP6A or PdPDLP6B restricted viral movement to the apical region. Scale bar = 5 cm. (e) CFDA dye loading on the adaxial side (upper panel) and fluorescence signal detected on the abaxial side (lower panel). Scale bar = 20 μm. (f) Statistics of relative CF dye diffusion area in (e). Values are means ± SD, n = 4, ** p < 0.01 (one-way ANOVA with Dunnett's test).

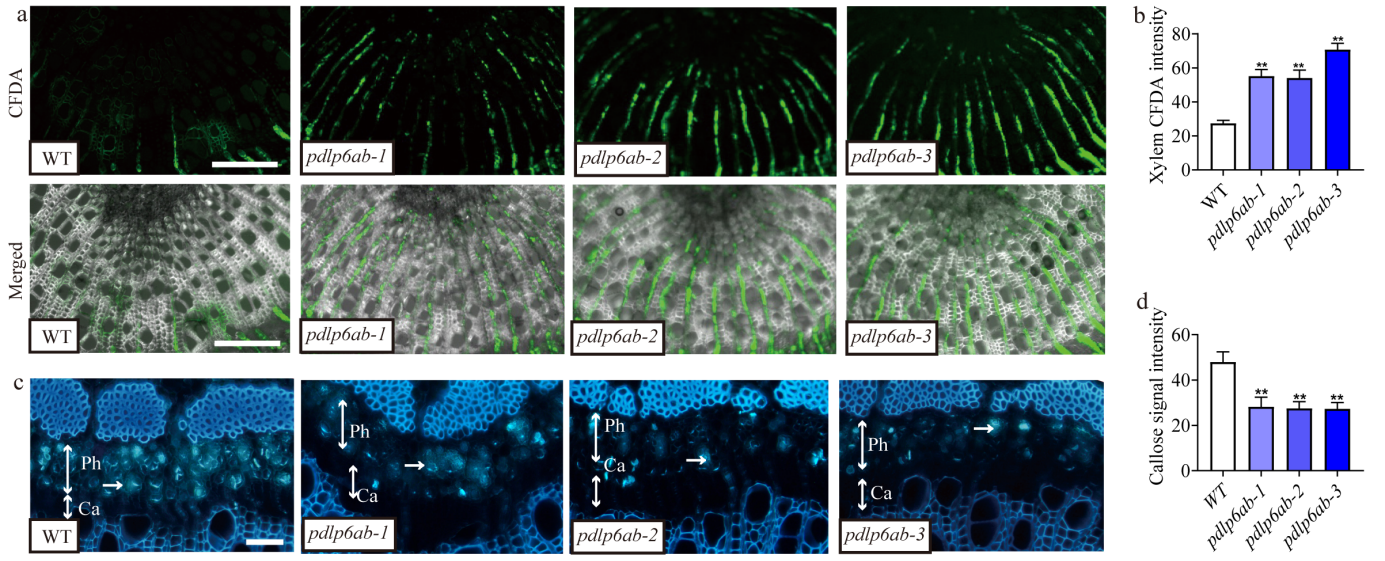


Fig. 6 Editing of *PdPDLP6A* and *PdPDLP6B* enhanced symplastic transport across the stem. (a) The fluorescent dye CFDA was used to examine symplastic transport in the *Populus* stem at the 14th internode. The fluorescence signal was detected in the xylem, indicating symplastic spread. Scale bar = 200 μm. (b) Quantification of the CF fluorescence signal intensity in (a). Values are means ± SD, n = 5, ** p < 0.01 (one-way ANOVA with Dunnett's test). (c) Callose stained by aniline blue was detected in the phloem and cambial zone of *Populus* stems at the 12th internode. Single-headed arrows indicate the stained callose, and two-headed arrows indicate the phloem and cambial zone. Ph, phloem; Ca, cambium. Scale bar = 20 μm. (d) Quantification of the callose fluorescence signal intensity in (c). Values are means ± SD, n = 5, ** p < 0.01 (one-way ANOVA with Dunnett's test).

Functional divergence of PDLP6 between *Arabidopsis* and *Populus*

The *Populus* genome encodes two PDLP6 homologs, whereas *Arabidopsis* contains a single PDLP6 gene. In *Arabidopsis*, the *pdlp6* single mutant does not show obvious growth defects[13]. However, TEM analysis revealed fewer starch grains in chloroplasts of mature leaves in the *pdlp6-1* mutant[13]. In addition, 35S-driven overexpression of *PDLP6* led to strong starch accumulation in mature leaves[13]. These observations suggest a role for *Arabidopsis PDLP6* in source leaf function. In *Populus*, single mutants of *PdPDLP6* show no visible phenotypes, while the double mutant exhibits a strong phenotype in stem secondary growth. Tissue expression analyses revealed

https://doi.org/10.48130/forres-0026-0033

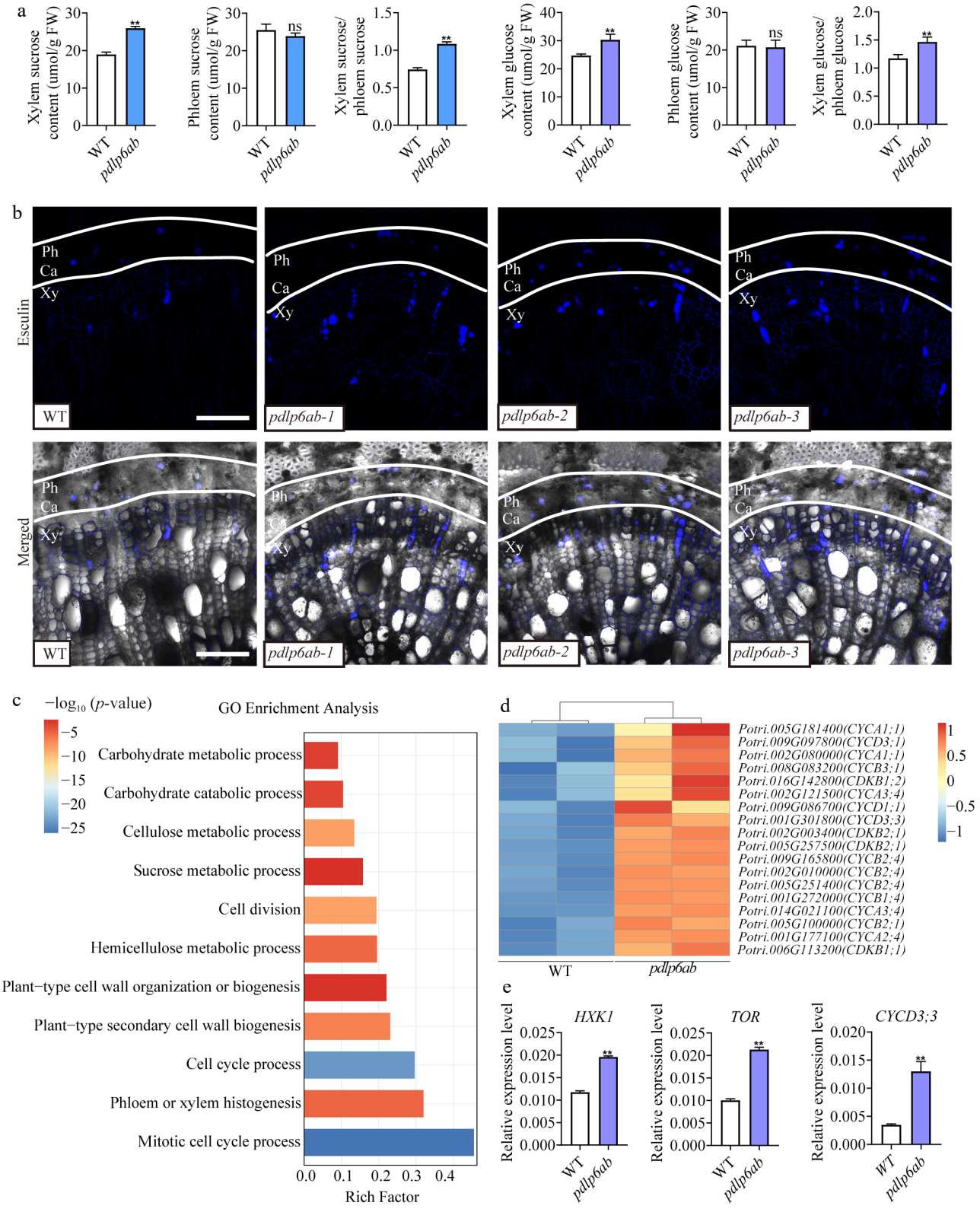


Fig. 7 Editing of *PdPDLP6A* and *PdPDLP6B* affects sugar transport. (a) Quantification of sucrose and glucose in the phloem and xylem of *Populus* stems at the 14th internode. Values are means ± SD, $n = 3$, ** $p < 0.01$ (Student's t-test). (b) The fluorescent sucrose analog esculin was used to visualize sucrose distribution in the *Populus* stems at the 14th internode. Ca, cambium; Ph, phloem; Xy, xylem. Scale bar = 100 μm. (c) GO enrichment analysis of differentially expressed genes (*pdlp6ab* vs WT). (d) The heatmap shows the relative expression of the cell cycle-related genes in WT and *pdlp6ab* plants. The color scale represents relative expression levels. (e) Relative expression levels of *HXK1*, *TOR*, and *CYCD3;3* determined by qRT-PCR. Values are means ± SD, $n = 3$ biological replicates per genotype, ** $p < 0.01$ (Student's t-test).

that both *PdPDLP6A* and *PdPDLP6B* are highly expressed in secondary stems but only weakly in leaves (Supplementary Fig. S6), indicating that in *Populus*, these genes function primarily in stem secondary growth.

These differences may reflect the distinct developmental patterns of the two species and their different source-sink transport requirements. *Arabidopsis* is a herbaceous plant that does not undergo continuous secondary growth. Photoassimilates produced in source leaves are primarily allocated to apical growth, flowering, and fruit development. *Populus*, in contrast, is a woody plant that undergoes extensive secondary growth. A substantial proportion of photoassimilates produced in leaves must be transported laterally into the stem to provide carbon for radial growth and xylem cell wall biosynthesis. PDLP6 duplication and the shift in expression pattern in *Populus* may reflect the demands of woody stem growth, which requires active radial symplastic transport from phloem to xylem. However, whether the functional divergence of PDLP6 is related to developmental differences between herbaceous and woody plants requires further investigation.

Conclusions

The PDLP family is known to regulate plasmodesmata-mediated symplastic transport. Here, we identified two PDLP6 homologs, *PdPDLP6A* and *PdPDLP6B*, in the *Populus* genome. The two homologs appear to function redundantly in regulating stem secondary growth in *Populus*. They colocalize with callose at plasmodesmata, affecting plasmodesmata-mediated symplastic transport across the stem, which is a key source–sink mechanism for secondary growth in trees. Our results indicate that PdPDLP6A and PdPDLP6B regulate symplastic transport during stem secondary growth in *Populus*.

Ethical statements

Not applicable.

Author contributions

The authors confirm their contributions to the paper as follows: study conception and design: Li L, Li R; draft manuscript preparation and analysis of results, data analysis: Li R, Qin H; performing the experiments and data collection: Li R, Qin H, Hu W, Luan K, Sun J, Shen J; manuscript modification: Li L. All authors reviewed the results and approved the final version of the manuscript.

Data availability

All data generated or analyzed during this study are included in this published article and its supplementary information files.

Acknowledgments

We thank Dr. Yaoguang Liu for providing the CRISPR/Cas9 vectors and Dr. Feng Li for providing *Agrobacterium tumefaciens* carrying *TMV-GFP*. We thank Wenjuan Cai for confocal laser scanning microscopy, Wenli Hu for GC–MS analysis, and Jiqin Li, Lina Xu, and Zhiping Zhang for transmission electron microscopy. This work was supported by the National Key Research and Development Program (2021YFD2200204), the Strategic Priority Research Program of the Chinese Academy of Sciences (XDB0630200), and the National Natural Science Foundation of China (32130072) awarded to LL.

Conflict of interest

The authors declare that they have no conflict of interest.

Supplementary information accompanies this paper online at: https://doi.org/10.48130/forres-0026-0033.

Dates

Received 6 June 2026; Revised 9 August 2026; Accepted 21 September 2026; Published online 23 October 2026

References

[1] Luo L, Li L. 2022. Molecular understanding of wood formation in trees. *Forestry Research* 2:5

[2] Plomion C, Leprovost G, Stokes A. 2001. Wood formation in trees. *Plant Physiology* 127:1513–1523

[3] Lu J, Wang Y, Wen Y, Ren Q, Wang Q, et al. 2025. A ray localized vacuolar sucrose transport is required for wood formation in *Populus tomentosa*. *The Plant Journal* 123:e70347

[4] Miras M, Pottier M, Schladt TM, Ejike JO, Redzich L, et al. 2022. Plasmodesmata and their role in assimilate translocation. *Journal of Plant Physiology* 270:153633

[5] Spicer R. 2014. Symplasmic networks in secondary vascular tissues: parenchyma distribution and activity supporting long-distance transport. *Journal of Experimental Botany* 65:1829–1848

[6] Roberts AG, Oparka KJ. 2003. Plasmodesmata and the control of symplastic transport. *Plant, Cell & Environment* 26:103–124

[7] Maule A, Faulkner C, Benitez-Alfonso Y. 2012. Plasmodesmata "in communicado". *Frontiers in Plant Science* 3:30

[8] Brunkard JO, Runkel AM, Zambryski PC. 2015. The cytosol must flow: intercellular transport through plasmodesmata. *Current Opinion in Cell Biology* 35:13–20

[9] Tilsner J, Nicolas W, Rosado A, Bayer EM. 2016. Staying tight: plasmodesmal membrane contact sites and the control of cell-to-cell connectivity in plants. *Annual Review of Plant Biology* 67:337–364

[10] Bayer EM, Benitez-Alfonso Y. 2024. Plasmodesmata: channels under pressure. *Annual Review of Plant Biology* 75:291–317

[11] Amsbury S, Kirk P, Benitez-Alfonso Y. 2017. Emerging models on the regulation of intercellular transport by plasmodesmata-associated callose. *Journal of Experimental Botany* 69:105–115

[12] Dominguez PG, Niittylä T. 2022. Mobile forms of carbon in trees: metabolism and transport. *Tree Physiology* 42:458–487

[13] Li Z, Liu SL, Montes-Serey C, Walley JW, Aung K. 2024. PLASMODESMATA-LOCATED PROTEIN 6 regulates plasmodesmal function in *Arabidopsis* vasculature. *The Plant Cell* 36:3543–3561

[14] Chen X, Li WW, Gao J, Wu Z, Du J, et al. 2024. *Arabidopsis* PDLP7 modulated plasmodesmata function is related to *BG10*-dependent glucosidase activity required for callose degradation. *Science Bulletin* 69:3075–3088

[15] Thomas CL, Bayer EM, Ritzenthaler C, Fernandez-Calvino L, Maule AJ. 2008. Specific targeting of a plasmodesmal protein affecting cell-to-cell communication. *PLoS Biology* 6:e7

[16] Sager R, Wang X, Hill K, Yoo BC, Caplan J, et al. 2020. Auxin-dependent control of a plasmodesmal regulator creates a negative feedback loop modulating lateral root emergence. *Nature Communications* 11:364

[17] Tamura K, Stecher G, Peterson D, Filipski A, Kumar S. 2013. MEGA6: molecular evolutionary genetics analysis version 6.0. *Molecular Biology and Evolution* 30:2725–2729

[18] Ma X, Zhang Q, Zhu Q, Liu W, Chen Y, et al. 2015. A robust CRISPR/Cas9 system for convenient, high-efficiency multiplex genome editing in monocot and dicot plants. *Molecular Plant* 8:1274–1284

[19] Li L, Zhou Y, Cheng X, Sun J, Marita JM, et al. 2003. Combinatorial modification of multiple lignin traits in trees through multigene cotransformation. *Proceedings of the National Academy of Sciences of the United States of America* 100:4939–4944

[20] Kaneda M, Rensing K, Samuels L. 2010. Secondary cell wall deposition in developing secondary xylem of poplar. *Journal of Integrative Plant Biology* 52:234–243
[21] Lindbo JA. 2007. TRBO: a high-efficiency tobacco mosaic virus RNA-based overexpression vector. *Plant Physiology* 145:1232–1240
[22] Herburger K, Holzinger A. 2016. Aniline blue and Calcofluor white staining of callose and cellulose in the streptophyte green algae *Zygnema* and *Klebsormidium*. *Bio-protocol* 6:e1969
[23] Mehdi R, Lamm CE, Bodampalli Anjanappa R, Müdsam C, Saeed M, et al. 2019. Symplasmic phloem unloading and radial post-phloem transport *via* vascular rays in tuberous roots of *Manihot esculenta*. *Journal of Experimental Botany* 70:5559–5573
[24] Kong Y, O'Neill M, Zhou G. 2018. Plant cell walls: isolation and monosaccharide composition analysis. *Methods in Molecular Biology* 1744:313–319
[25] Li R, Wang Z, Wang JW, Li L. 2023. Combining single-cell RNA sequencing with spatial transcriptome analysis reveals dynamic molecular maps of cambium differentiation in the primary and secondary growth of trees. *Plant Communications* 4:100665
[26] Knox JP, Benitez-Alfonso Y. 2014. Roles and regulation of plant cell walls surrounding plasmodesmata. *Current Opinion in Plant Biology* 22:93–100
[27] Collins C, Maruthi NM, Jahn CE. 2015. *CYCD3* D-type cyclins regulate cambial cell proliferation and secondary growth in *Arabidopsis*. *Journal of Experimental Botany* 66:4595–4606
[28] Guan C, Xue Y, Jiang P, He C, Zhuge X, et al. 2021. Overexpression of *PtoCYCD3;3* Promotes Growth and Causes Leaf Wrinkle and Branch Appearance in *Populus*. *International Journal of Molecular Sciences* 22(3):1288
[29] Riou-Khamlichi C, Menges M, Healy JM, Murray JA. 2000. Sugar control of the plant cell cycle: differential regulation of *Arabidopsis* D-type cyclin gene expression. *Molecular and Cellular Biology* 20:4513–4521
[30] Díaz-Granados VH, López-López JM, Flores-Sánchez J, Olguin-Alor R, Bedoya-López A, et al. 2020. Glucose modulates proliferation in root apical meristems *via* TOR in maize during germination. *Plant Physiology and Biochemistry* 155:126–135
[31] Saatian B, Kohalmi SE, Cui Y. 2023. Localization of *Arabidopsis* Glucan Synthase-Like 5, 8, and 12 to plasmodesmata and the GSL8-dependent role of PDLP5 in regulating plasmodesmal permeability. *Plant Signaling & Behavior* 18:2164670
[32] Vatén A, Dettmer J, Wu S, Stierhof YD, Miyashima S, et al. 2011. Callose biosynthesis regulates symplastic trafficking during root development. *Developmental Cell* 21:1144–1155

Copyright: © 2026 by the author(s). Published by Maximum Academic Press, Fayetteville, GA. This article is an open access article distributed under Creative Commons Attribution License (CC BY 4.0), visit https://creativecommons.org/licenses/by/4.0/.